

# Ultrashort pulse non-linear optical absorption in transparent media

D. M. Rayner, A. Naumov and P. B. Corkum

Steacie Institute for Molecular Science, National Research Council, 100 Sussex Drive,  
Ottawa, Ontario K1A 0R6, Canada

[david.rayner@nrc-crnc.gc.ca](mailto:david.rayner@nrc-crnc.gc.ca); [paul.corkum@nrc-crnc.gc.ca](mailto:paul.corkum@nrc-crnc.gc.ca)

**Abstract:** A focused ultrashort pulse can reach high enough intensity that non-linear ionization dominates its interaction with transparent media while still having relatively low fluence. In this case, the energy extracted from the beam can counter self-focusing by energy depletion and plasma formation, providing controlled energy deposition that can modify the material in a highly local manner. We demonstrate that non-linear absorption limits the intensity that can be reached and that the energy is deposited prior to the focus. We model the energy distribution, and predict and measure the energy transmitted through the focus. We establish the threshold intensity for non-linear ionization in dielectrics at  $\sim 10^{13}$  W cm $^{-2}$ . We use the refractive index modification that the non-linear ionization causes in glass to image the spatial distribution of the energy deposition.

© 2005 Optical Society of America

**OCIS codes:** (190.4180) Multiphoton processes; (320.7110) Ultrafast nonlinear optics

---

## References and links

1. K. M. Davis, K. Miura, N. Suguimoto, and K. Hirao, "Writing waveguides in glass with a femtosecond laser," *Opt. Lett.* **21**, 1729–1731 (1996).
2. A. M. Streltsov and N. F. Borrelli, "Study of femtosecond-laser-written waveguides in glasses," *J. Opt. Soc. Am. B* **19**, 2496–2504 (2002).
3. V. R. Bhardwaj, P. B. Corkum, D. M. Rayner, C. Hnatovsky, E. Simova, and R. S. Taylor, "Stress in femtosecond-laser-written waveguides in fused silica," *Opt. Lett.* **29**, 1312–1314 (2004).
4. R. S. Taylor, C. Hnatovsky, E. Simova, D. M. Rayner, V. R. Bhardwaj, and P. B. Corkum, "Femtosecond laser fabrication of nanostructures in silica glass," *Opt. Lett.* **28**, 1043–1045 (2003).
5. A. Marcinkevičius, S. Juodkaziš, M. Watanabe, M. Miwa, S. Matsuo, and H. Misawa, "Femtosecond laser-assisted three-dimensional microfabrication in silica," *Opt. Lett.* **26**, 277–279 (2001).
6. N. Shen, C. B. Schaffer, D. Datta, and E. Mazur, "Photodisruption in biological tissues and single cells using femtosecond laser pulses," in *Conference on Lasers and Electro-Optics*, pp. 403–404 (Baltimore, MD, 2001).
7. M. F. Yanik, H. Cinar, H. N. Cinar, A. D. Chisholm, Y. Jin, and A. Ben-Yakar, "Neurosurgery: Functional regeneration after laser axotomy," *Nature* **432**, 822 (2004).
8. V. Keldysh, "Ionization in the field of a strong electromagnetic wave," *Sov. Phys. JETP* **20**, 1307–1314 (1965).
9. D. von der Linde and H. Schüller, "Breakdown threshold and plasma formation in femtosecond laser-solid interaction," *J. Opt. Soc. Am. B* **13**, 216–222 (1996).
10. J. Krüger and W. Kautek, "Femtosecond-pulse visible laser processing of transparent materials," *Appl. Surf. Sci.* **96-98**, 430–438 (1996).
11. S. Augst, D. Strickland, D. D. Meyerhofer, S. L. Chin, and J. H. Eberly, "Tunneling ionization of noble gases in a high-intensity laser field," *Phys. Rev. Lett.* **63**, 2212–2215 (1989).
12. P. B. Corkum, C. Rolland, and T. Srinivasan-Rao, "Supercontinuum generation in gases," *Phys. Rev. Lett.* **57**, 2268–2271 (1986).
13. O. M. Efimov, L. B. Glebov, S. Grantham, and M. Richardson, "Photoionization of silicate glasses exposed to IR femtosecond pulses," *J. Non-crystal. Solids* **253**, 58–67 (1999).

14. A. Vogel, J. Noack, K. Nahen, D. Theisen, S. Busch, U. Parltitz, D. Hammer, G. Noojin, B. Rockwell, and R. Birngruber, "Energy balance of optical breakdown in water at nanosecond to femtosecond time scales," *Appl. Phys. B* **68**, 271–280 (1999).
  15. L. N. Gaier, M. Lein, M. I. Stockman, P. L. Knight, P. B. Corkum, M. Y. Ivanov, and G. L. Yudin, "Ultrafast multiphoton forest fires and fractals in clusters and dielectrics," *J. Phys. B: At. Mol. Phys.* **37**, L57–L67 (2004).
  16. G. L. Yudin, L. N. Gaier, M. Lein, P. L. Knight, P. B. Corkum, and M. Y. Ivanov, "Hole-Assisted Energy Deposition in Clusters and Dielectrics in Multiphoton Regime," *Laser Physics* **14**, 51–56 (2004).
  17. W. Liu, S. Petit, A. Becker, N. Aközbeke, C. M. Bowden, S. L. Chin, "Intensity clamping of a femtosecond laser pulse in condensed matter," *Opt. Commun.* **202**, 189–197 (2002).
  18. M. Lenzner, J. Krger, S. Sartania, Z. Cheng, C. Spielmann, G. Mourou, W. Kautek, and F. Krausz, "Femtosecond Optical Breakdown in Dielectrics," *Phys. Rev. Lett.* **80**, 4076–4079 (1998).
- 

## 1. Introduction

Energy deposition at the focus of an intense laser beam in transparent condensed phase material is a central issue in applications that range from photonics fabrication to materials science and from biology to medicine. At modest intensities, such as those used for two-photon microscopy and CARS microscopy, only a small percentage of the light is absorbed and the focal parameters, and hence the intensity, range and position of the interaction volume can be obtained from the standard beam propagation formulae. This is not the case when tightly focused femtosecond laser beams reach the intensities required to drive highly non-linear absorption, typically with the purpose of depositing enough energy to modify the material locally. Examples include: femtosecond dielectric modification, where femtosecond lasers focused in substrates such as fused silica are used to change the refractive index of the material on a micrometre scale to write waveguides and possibly provide a technology for 3-D photonics [1, 2, 3]; femtosecond laser 3-D patterning as a precursor for selective chemical etching of microstructures and microfluidic channels [4, 5]; femtosecond laser microsurgery both as a tool for biological research and as a possible medical procedure [6, 7]. In these applications it is necessary to absorb a significant portion of the short, low energy laser pulse in order to drive chemical reaction and structural change. This absorption must be considered when considering the beam propagation and mapping out the deposited energy distributions.

We show that, in the condensed phase, the deposited energy density (and hence the plasma density in the case of multi-photon ionization) is limited by depletion of the laser beam (running out of photons). In contrast, in the gas phase the absorption is limited by running out of material. We develop and test a simple analytical model for the propagation of a focused, non-resonant, Gaussian beam in a strongly non-linear absorbing medium. This model highlights the self-control of the laser-material interaction, predicts the total absorption and allows calculation of deposited energy distributions. An important concept that emerges from the model is that non-linear absorption provides a self-control mechanism for the interaction. The absorption clamps the applied maximum intensity in the material close to the threshold intensity, even for pulses that, when similarly focused in air, would reach intensities much higher than the threshold.

The control allows efficient and controllable energy deposition even when the nominal pulse power exceeds the self focusing threshold. This is because significant changes to the beam due to self-focusing and self-phase modulation require the accumulated phase retardation  $\delta\phi$ , due to the non-linear index-of-refraction and given by  $2\pi \int \eta_2 E^2 dl / \lambda$ , to exceed  $\pi$ . If the path length is small, the integral can only become large if  $E^2$  becomes large. High-order effects can dominate before this happens. In this limit the magnitude of the laser field is restricted by non-linear absorption and so the integral can not become large. Neither temporal or spatial collapse is possible. We measure the transmitted spectrum showing that there is little spectral broadening. Since self-focusing and self-phase modulation are related phenomena, this is a direct measure that self-focusing does not occur.

We use dielectric modification in silica glasses to demonstrate this controlled energy deposi-

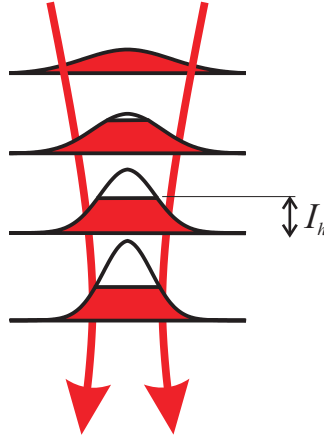


Fig. 1. Self-limitation of non-linear absorption of a focused laser beam in transparent dielectric material. The intensity dependence of a highly non-linear absorption is approximated by a step function. Far from the focus absorption is negligible because the intensity is below the threshold for non-linear absorption,  $I_h$ . As the beam approaches the focus and  $I_h$  is exceeded the intensity is clamped at  $I_h$  energy is removed from the beam.

tion. The characteristics of silica are typical of many dielectrics. The self-focusing power is on the order of 2.5 MW. For a 40 fs pulse this corresponds to a pulse energy of 100 nJ. In the absence of non-linear absorption with a 0.25 NA lens the focused intensity can approach  $3 \times 10^{13}$  W cm<sup>2</sup> before catastrophic collapse of the beam. We will show that non-linear absorption begins at  $10^{13}$  W cm<sup>-2</sup>, essentially the threshold predicted by Keldysh theory of multi-photon ionization in gases and solids[8]. With the intensity capped at  $10^{13}$  W cm<sup>-2</sup> self-focusing is not possible even when self-focusing threshold is nominally exceeded.

## 2. Self-limiting absorption

Our model is developed for cases where high order non-linear ionization is the dominant non-linear mechanism. Since it requires many photons to supply the band gap energy in transparent material we approximate non-linear absorption with a threshold (step function). Although a convenient assumption, any highly non-linear process will give essentially the same results. The essence of the process is depicted in Fig. 1 and can be appreciated by assuming that intensities above a threshold intensity,  $I_h$ , are absorbed and the pulse is modified, “trimmed”, in time and spatial distribution by this process as it propagates through the focus. That is, the peak intensity of the pulse, which would otherwise grow as it approaches the focus, according to the confocal parameters, is continually trimmed to a flat top of intensity  $I_h$ . The total energy absorbed can be obtained first, without needing to consider the spatial distribution. Although energy is absorbed before the focus, the final cut is made at the focal plane. The total absorption is therefore equivalent to that derived as if the pulse reaches the focal plane unattenuated and is absorbed there. For a spatial and temporal Gaussian pulse, maximum intensity  $I_0$ , radius (at 1/e)  $\omega_0$  and half pulse width  $\tau$  (at 1/e) the absorption rate at time  $t$  during the pulse,  $dE_A/dt$ , is given by

$$\frac{dE_A}{dt} = \pi\omega_0^2(I_0e^{-t^2/\tau^2} - I_h) - \pi r_h^2 I_h. \quad (1)$$

The first term on the right hand side is the incident power out to the radius  $r_h$  at which  $I = I_h$ . The second term is the portion of this power that is transmitted under the step-function threshold.

Substituting for  $r_h^2$ , given by  $\omega_0^2 \ln(I_0 \exp(-t^2/\tau^2)/I_h)$ , we find

$$\frac{dE_A}{dt} = \pi \omega_0^2 e^{-t^2/\tau^2} \left\{ 1 - \frac{I_h}{I_0 e^{-t^2/\tau^2}} \left( 1 + \ln \frac{I_0 e^{-t^2/\tau^2}}{I_h} \right) \right\}. \quad (2)$$

Integration over time gives the total energy absorbed as

$$E_A = E_0 \left\{ \operatorname{erf} \left( \sqrt{\ln \frac{I_0}{I_h}} \right) - \frac{2}{\pi} \frac{I_h}{I_0} \left( 1 + \frac{2}{3} \ln \frac{I_0}{I_h} \right) \sqrt{\ln \frac{I_0}{I_h}} \right\}. \quad (3)$$

where  $E_0$  is the incident pulse energy  $= \pi^{2/3} \omega_0^2 \tau I_0$ .

The spatial distribution of the absorbed energy requires more detailed consideration. We assume that a topped Gaussian pulse maintains a Gaussian profile in the wings as it comes to a focus so that the intensity is determined by

$$I(z, r, t) = \frac{I_0}{1 + z^2/z_0^2} \exp - \frac{r^2}{\omega_0^2 (1 + z^2/z_0^2)} \exp - \frac{t^2}{\tau^2} \quad (4)$$

for  $r > r'$ , the radius at which  $I(z, r, t) = I'$ , the plateau intensity. Here  $z$  is the distance from the focal plane,  $r$  is the distance from the beam axis and  $z_0$  is the Raleigh length. Under these conditions, and in the absence of adsorption,  $I'$  increases with  $z$  according to

$$\frac{\partial I'}{\partial z} = \frac{2z}{z_0^2 + z^2} I'. \quad (5)$$

Under the step-function model the plateau intensity is clamped at  $I_h$  so that the absorption rate,  $\partial I_a / \partial z$ ,  $= \partial I' / \partial z$  with  $I' = I_h$ , *i.e.*

$$\begin{aligned} \frac{\partial I_a}{\partial z} &= \frac{2z}{z_0^2 + z^2} I_h & [r < r_h; -t_h < t < t_h] \\ &= 0 & [r \geq r_h; t \geq |t_h|]. \end{aligned} \quad (6)$$

The limits  $r_h$  and  $t_h$  are respectively the radius and time at which  $I(z, r, t) = I_h$ . The absorption rate depends only on  $I_h$  and  $z$ . At a chosen radius,  $r < r_h$ , Eq. (6) applies over the period from  $-t_h$  to  $t_h$  where  $I(z, r, t) \geq I_h$ . The absorbed energy density,  $N(z, r)$ , is then identified as  $2t_h \partial I_a / \partial z$ .

With  $t_h$  obtained from Eq. (4), with  $I(z, r, t_h) = I_h$  the absorbed energy density is determined as

$$N(z, r) = \frac{-4I_h \tau z}{z_0^2 + z^2} \sqrt{\ln \left( \frac{I_0}{I_h \left( 1 + \frac{z^2}{z_0^2} \right)} \right) - \frac{r^2}{\omega_0^2 \left( 1 + \frac{z^2}{z_0^2} \right)}}. \quad (7)$$

Integration of this expression over  $z$  and  $r$  leads to the same result for  $E_A$  as Eq. (3), as expected.

The maximum energy density,  $N_{max}$ , is located on the beam axis at  $z_{max}$  where the condition

$$\ln \left( \frac{I_0}{I_h \left( 1 + \frac{z_{max}^2}{z_0^2} \right)} \right) = \frac{z_{max}^2}{(z_0^2 - z_{max}^2)} \quad (8)$$

is satisfied. Setting  $z = z_{max}$  and  $r = 0$  in Eq. 7 gives  $N_{max}$ . Inspection of Eq. 8 shows that the ratio  $z_{max}/z_0$  depends only on the ratio  $I_0/I_h$ . The maximum energy density is always found between  $z = 0$  and  $z = z_0$ , with  $z_{max} \rightarrow 0$  when  $I_0/I_h \rightarrow 1$  and  $z_{max} \rightarrow z_0$  as  $I_0/I_h \rightarrow \infty$ .

We perform numerical analysis to investigate more complex ionization mechanisms than a step-function. The absorption model relates  $dI/dt$  and  $dn/dt$  to  $I$  and  $n$ , where  $n$  is the carrier density. We assume the modified pulse propagates as a Gaussian, as in the analytical solution, and follow  $n(z, r, t)$  and  $I(z, r, t)$  by forward integration, starting at a negative value of  $z$  where absorption is insignificant. Specific ionization mechanisms we have considered are multiphoton ionization, where  $dn/dt = \sigma_k I^k$  with  $k$  the multiphoton order, multiphoton ionization plus avalanche ionization, where  $dn/dt = \sigma_k I^k + \alpha n I$  with  $\alpha$  the avalanche coefficient, and tunnel ionization where  $dn/dt$  is given by the Keldysh formulation [8].

### 3. Experimental

Optical pulses for the experiments were obtained from a Coherent RegA 9050 regenerative amplifier combined with home-build Ti:Sapphire oscillator, stretcher and compressor. The repetition rate of the amplifier was controlled via computer interface and could be varied from single shot to 250 kHz. The maximum energy of the laser pulse that could be delivered to a target was to 3  $\mu\text{J}$ . The 50 fs pulse duration was measured with autocorrelator or FROG. The beam intensity was varied using a set of neutral density reflective filters with optical density up to 3. The laser beam was focused with a regular refractive 10 $\times$  microscope objective with numeric aperture, NA, 0.25. The light after the sample was collected with matching objective and directed to CCD camera, power meter, photodetector or spectrometer. For non-linear transmission measurements the second microscope objective was removed and a photodetector with an active size of 10 mm in diameter was placed directly behind the sample.

All experiments were carried out in air with the glass samples mounted on a motorized computer-controlled XYZ translation stage with minimum translation step of 0.1  $\mu\text{m}$  and maximum translation speed of 200  $\mu\text{m/s}$ . Images of material modification were obtained with an optical microscope equipped with a CCD camera. To determine the transmitted energy the laser beam was first focused in front of the sample, near the surface, but so that no surface ablation was observed. Then, the shutter was opened for a short period of time and a sample was exposed to a set number of laser pulses. Then the shutter was closed and the sample was moved 5  $\mu\text{m}$  towards the microscope objective and 10  $\mu\text{m}$  perpendicular to the optical axis. The sample was then exposed to the same number of laser pulses. This procedure was repeated until the focus emerged from the other side of the sample.

The quality of the focal spot was monitored with a CCD camera when the fs laser beam was focused at the same spot as the reference He-Ne laser beam. In this way we can compare the intensity profiles of the femtosecond with the He Ne beam. The intensity profiles of both laser beams was Gaussian with full-width at 1/e in the intensity of 2.8  $\mu\text{m}$  and 3.2  $\mu\text{m}$  for He-Ne and fs laser beams respectively. The highest pump intensity was  $\sim 8 \times 10^{14} \text{ W cm}^{-2}$ . This intensity is high enough to create a surface plasma and cause ablation of most materials [9, 10] as well as ionization of most gases [11]. The experimental layout allowed us to observe modifications of the beam profile after propagation through the glass sample due to self-focusing effects or internal/surface material modification.

### 4. Transmission measurements

Figure 2(a) shows the transmitted energy as a function of the distance between the beam waist and the front surface of a 0.8 mm thick Pyrex sample.

A sharp decrease in transmission near the front surface at high intensities corresponds to surface plasma formation and nearly complete absorption of the laser pulse at the surface. When the focus is inside the sample, intensity dependent absorption is observed. As the focus moves outside the sample at 800  $\mu\text{m}$ , 100% transmission is recovered. As can be seen from Fig. 2(b), absorption in the bulk is strongly non-linear and starts to saturate at pulse energies of

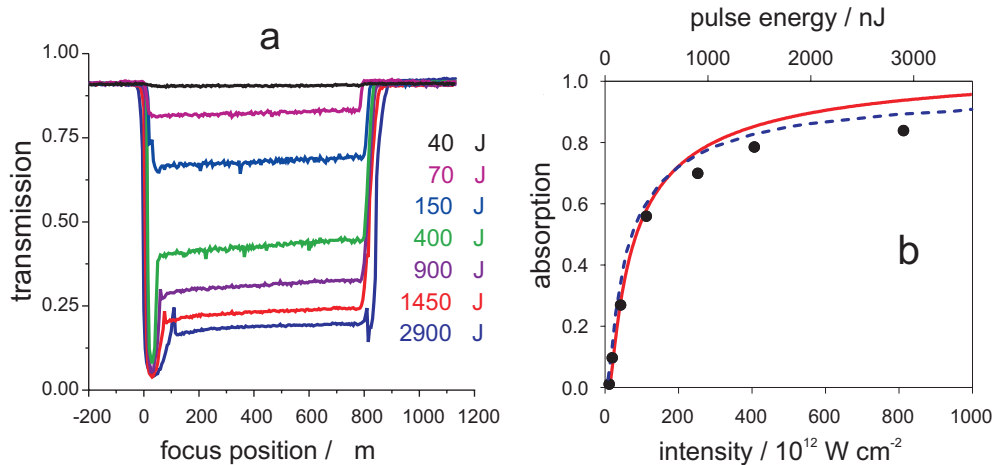


Fig. 2. a) Transmission of a high intensity femtosecond laser pulse through a 0.8 mm thick Pyrex sample as a function of focal position for a range of pulse energies. b) Adsorption when the focus was centered in the sample as a function of intensity. The points are the experimental measurements and the solid line is the result of the model described in the text with the threshold intensity,  $I_h$  set at  $9.8 \times 10^{12} \text{ W cm}^{-2}$ . The dashed curve is obtained by numerical analysis using the ionization probabilities predicted by Keldysh theory for Pyrex glass (Bandgap  $\approx 4.5 \text{ eV}$ ). In all cases the sample was moved orthogonally to the laser beam to expose a fresh volume of the sample on every shot.

about  $2 \mu\text{J}$ , which corresponds to an intensity of  $5.6 \times 10^{14} \text{ W cm}^{-2}$ . The transmission losses are nearly independent on the position inside the sample. Since the linear absorption in this spectral region is negligible, multiphoton absorption is almost certainly the main reason for transmission losses. Fig. 2(b) plots the bulk absorption as a function of the laser pulse energy. The absorption rises rapidly, before saturating at high energy. Internal absorption commences at an intensity that is very close to the 40 nJ threshold for surface damage (not shown). The intensity of the beam at threshold is approximately  $1.1 \times 10^{13} \text{ W cm}^{-2}$ .

Before discussing this data, we must demonstrate that the beam is not undergoing catastrophic self-focusing. We estimate the critical power for self-focusing occurs for an energy of about 100 nJ, an energy at which there is already strong absorption. To confirm this interpretation we study the transmitted spectrum. Supercontinuum generation and self-focusing are closely related phenomena. Therefore, if the spectrum is not broadened very much, self-phase modulation and self-focusing must play a limited role in the experiment. Figure 3 shows the transmitted spectrum, and compares it with the incident spectrum. The spectrum of the transmitted pulse (solid lines) is asymmetrically broadened with respect to the incident radiation (dotted lines) and shifted predominantly to the blue. Blue spectral shifts are characteristic of plasma formation as is the relatively small increase in the bandwidth that is observed in the figure [12].

The solid line in Fig. 2(b) is the result of fitting the lower intensity adsorption results for Pyrex glass to Eq. (3) by varying  $I_h$ . We find  $I_h = 9.8 \times 10^{12} \text{ W cm}^{-2}$ . It corresponds to an experimental threshold energy of 35 nJ. This is close to the approximate value obtained above by inspection of the data. The model fits the results well up to intensities of  $\sim 10^{14} \text{ W cm}^{-2}$  ( $\sim 400 \text{ nJ/pulse}$ ) or  $10 \times I_h$ . We attribute the departure at high intensities to the effect of plasma defocussing which deviates the beam and lowers the intensity available for absorption.

We have also used numerical analysis to address the adequacy of the simple threshold model.

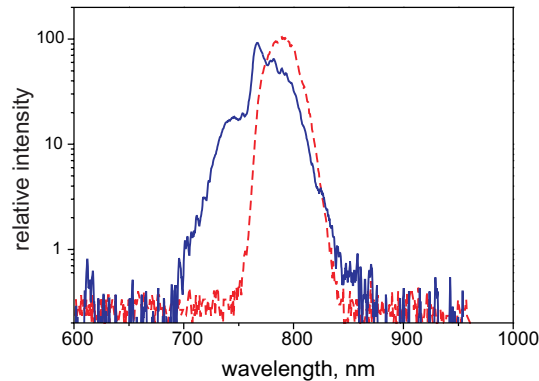


Fig. 3. Spectrum of a femtosecond laser pulse ( $1.5 \mu\text{J}$ , 40 fs) following transmission through a focus (NA 0.25) in fused silica (blue curve). The 37 MW pulse contains 15 times the critical power for self-focusing. The red curve shows the spectrum of the pulse prior to entering the sample.

We find that the model provides an adequate description where the threshold is not absolutely abrupt, for instance in the case of an intensity power dependence. The dashed curve in Fig. 2(b) is obtained by numerical analysis using the ionization probabilities predicted by Keldysh theory for Pyrex glass[8]. Clearly, when self-limiting absorption is taken into account, Keldysh theory describes the ionization of the dielectric well.

We can also include avalanche ionization through numerical analysis. Although there are small differences in the predicted free carrier spatial distributions, the adsorption process is self-limiting regardless of the details of the mechanism. Any highly non-linear process – avalanche, multiphoton ionization, tunneling or forest fires – yield qualitatively the same results. All are governed by depletion.

## 5. Deposited energy density profiles

Figure 4 shows typical deposited energy density profiles predicted by our model for highly non-linear absorption as given by Eq. (7). The conditions are typical for absorption of 800 nm light in glasses but are also expected to apply to liquids such as water that have similar band gaps and therefore similar ionization thresholds. Several points emerge from this analysis: i) the self-limiting nature of the adsorption process is evident from the maximum absorbed energy density, which, for instance, only increased by a factor of 2.4 when the pulse energy increased by a factor of 10 from 0.1 to  $1 \mu\text{J}$ ; ii) the maximum energy density point is located before the focus; iii) the energy density distribution, and therefore the interaction region, is foreshortened in the z-direction compared to the intensity distribution in the unmodified beam through the focus; iv) at a pulse energy of 100 nJ, the energy which corresponds to the critical power for self-focusing, the model predicts energy densities of up to  $250 \text{ J cm}^{-3}$ . This corresponds to carrier densities of up to  $1.7 \times 10^{20} \text{ cm}^{-2}$  ( $\approx 1/10$  the critical density) for a 6 photon band gap material showing that plasma formation is well established before this limit is reached; v) for the same laser conditions, material that has a higher ionization threshold can experience higher maximum carrier densities, if  $I_h$  is exceeded before the focus. This is contrary to the intuition that the easier to ionize material should show the higher maximum absorbed energy density. The last point is emphasized by Fig. 5 that shows the dependence of the maximum energy density,  $N_{max}$ , on the pulse energy for a series of threshold intensities.

Femtosecond laser dielectric modification provides a further qualitative test of the concepts

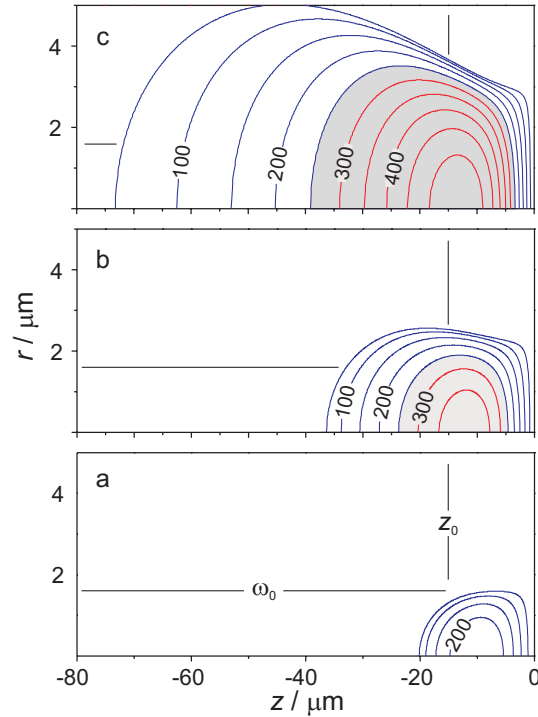


Fig. 4. Modelled energy distributions following highly non-linear absorption of a focused, short-pulse laser beam in dielectric material at pulse energies of (a) 100 nJ, (b) 250 nJ and (c) 1000 nJ. The contours are at  $50 \text{ J cm}^{-3}$  intervals. The distributions are over  $z$ , the distance from the nominal focal plane, and  $r$ , the radial distance from the beam axis. With a pulse duration of 50 fs (full width at  $1/e$ ) and a beam radius,  $\omega_0$ , of  $1.6 \mu\text{m}$  the corresponding peak intensities are (a)  $2.8 \times 10^{13} \text{ W cm}^{-2}$ , (b)  $7 \times 10^{13} \text{ W cm}^{-2}$  and (c)  $28 \times 10^{13} \text{ W cm}^{-2}$ . The threshold intensity was  $0.98 \times 10^{13} \text{ W cm}^{-2}$  corresponding to an energy threshold of 35 nJ. These are the threshold and beam parameters used to model the experimental transmission results in Fig. 2. The shaded areas mark regions where the energy density is  $> 250 \text{ J cm}^{-3}$ . At 800 nm this is equivalent to an absorption of  $10^{21}$  photons per  $\text{cm}^3$  and creation of a carriers density of  $\sim 1/10$  the critical density.

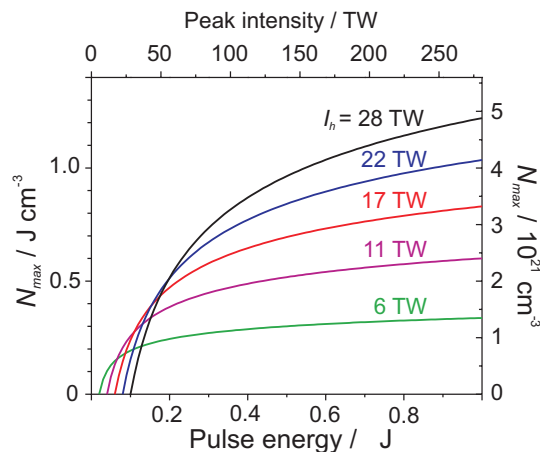


Fig. 5. Modelled peak energy densities,  $N_{max}$ , as a function of peak focused laser pulse intensity (top scale) or pulse energy (bottom scale) for several threshold intensities,  $I_h$ . The right scale gives the density in terms of photons absorbed. The laser pulse has the same characteristics as in Fig. 4.

behind the self-limiting model for highly non-linear absorption. We have taken advantage of this process to compare the region of refractive index modification in BK7 glass with the spatial energy distribution predicted by the model. Fig. 6 shows a transmission optical micrograph of the region of refractive index modification following femtosecond laser irradiation of BK7 glass. It is clear that the energy deposition is asymmetric about the focal plane with a larger volume being modified on the side nearer the laser as predicted. The bright spot in the image corresponds to the volume close to the focus where sufficient energy is deposited to cause refractive index modification. The darkening further from the focus is thought to be due to colour centre formation which occurs following low-level free carrier generation in certain glasses at intermediate energies [13].

Also shown in Fig. 6 are contour plots of the free carrier density predicted by the model. There is a strong correspondence between the shape of the modified volume and the plasma density as predicted by the model. This is another clear demonstration of the self-limiting and controlled nature of the absorption process. Our model is also consistent with studies of optical breakdown and bubble formation in water due to a 100 fs laser pulse [14]. Images of the breakdown region made using a laser flash photography Schlieren technique show heating of the liquid upstream of the zone where the bubble is produced that is consistent with the energy distributions we predict.

## 6. Conclusions

Our model is based on two approximations. First, we assume that the focal distribution of a Gaussian beam is only modified by attenuation, not by diffractive effects. This is adequate for small attenuation, but the model would be improved by taking diffraction into account when the attenuation becomes large. Second we assume that highly non-linear absorption can be approximated by a step function.

However, the qualitative conclusion that self-focusing is overwhelmed by nonlinear absorption for small F# beams is not sensitive to either of these assumptions. Self-focusing will be controlled if absorption is caused by multiphoton ionization, avalanche ionization, or multi-

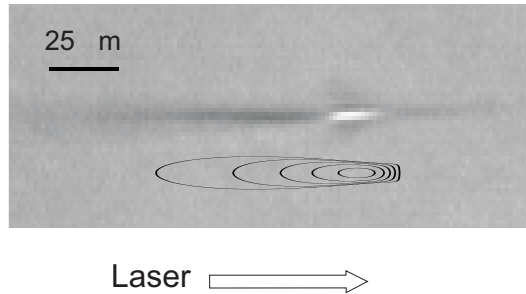


Fig. 6. Optical micrograph showing modification inside BK7 glass by a  $1.3 \mu\text{J}$ , 50 fs FWHM femtosecond laser pulse. To increase contrast in the micrograph a stack of 50 single shots made at a spacing of  $4 \mu\text{m}$  is viewed from the side. The beam diameter was  $3.2 \mu\text{m}$  so there is little overlap between the shots, especially at the focus. The contours depict the plasma density as predicted by the non-linear adsorption model described in the text. The contours are at densities from  $0.8 \times 10^{20}$  to  $7.5 \times 10^{20} \text{ cm}^{-3}$  in steps of  $1.7 \times 10^{20} \text{ cm}^{-3}$  and are offset from the laser axis for clarity.

photon "forest fires" [15, 16]]. Likewise the self-limiting nature of absorption is insensitive to model details. Energy will not make it past the pre-focal region, forcing the deposition before the focus. Only details of the distribution in Fig. 4 will change.

Self-focussing will play a role for larger F# beams. Characteristics of short pulse self-focussing will contribute to the energy distribution. For example, the beam focus will sweep through the pre-focal region and continuum light will be generated. However, even then non-linear absorption will prevent beam collapse because of depletion or plasma defocussing [17].

There are two important further issues that arise out of work. First, contrary to recent claims [18] our results show that dielectrics ionize at the threshold given by tunnelling theory. In other words, ionization is not suppressed in silica. Second, the pulse duration is an important control parameter. The deposited energy distribution is directly proportional to the pulse duration. Our experiment was performed with 50 fs pulses. If we had used 5 fs pulses, the absorbed energy densities in Fig. 4 would have been one order of magnitude lower. Laser pulse duration is an important control parameter for dielectrics.